J. Nano- Electron. Phys.
3 (2011) No1, P.170-178

PACS numbers: 61.46.Hk, 81.07.Bc

OXIDE NANOSTRUCTURES: CHARACTERIZATIONS AND OPTICAL BANDGAP EVALUATIONS OF COBALT-MANGANESE AND NICKEL-MANGANESE AT DIFFERENT TEMPERATURES

***C.R. Indulal*[1], *G.S. Kumar*[1], *A.V. Vaidyan*[2], *R. Raveendran*[1]**

[1] Department of Physics,
S N College, Kollam, India
E-mail: cr_indulal@yahoo.com

[2] Department of Chemistry,
St Stephens College, Pathanapuram, India

Cobalt-Manganese and Nickel-Manganese oxide (CoMnO and NiMnO) nanoparticles were prepared by chemical co-precipitation method by decomposition of their respective metal sulfides and sodium carbonate using ethylene diamene tetra acetic acid as the capping agent. The samples were heated at 400, 600 *and* 800 °*C. The average particle sizes were determined from the X-ray line broadening. The diffractograms were compared with JCPDS data to identify the crystallographic phase and cubic structure of the particles. The samples were characterized by XRD, FTIR and UV analyses. The internal elastic micro strains were calculated and it was seen that as the particle size increases strain decreases. The FTIR studies have been used to confirm the metal oxide formation. The chemical compositions of the samples were verified using EDX spectra. The surface morphologies of the samples were studied from the SEM images. The absorption spectra of the materials in the UV-Vis-NIR range were recorded. From the analysis of the absorption spectra, the direct band gaps of the materials were calculated.*

Keywords: *NANOPARTICLES, ARRESTED PRECIPITATION, SEM, EDX, OPTICAL BAND GAP.*

(Received 04 February 2011, in final form 18 March 2011)

1. INTRODUCTION

Recently nano oxide particles have been drawing much attention because of their peculiar optical [1, 2] and magnetic [3] properties. Due to the large surface to volume ratio of nano particles, their properties (electrical, optical, chemical, mechanical and magnetic) can be selectively controlled by engineering the size, morphology and composition of the particles. Nano crystalline materials exhibiting this large surface area can be applied to gas sensors for which an excellent surface effect is required. These new assemblies can have enhanced or entirely different properties from their parent bulk materials [4].The fine particles of the compounds with very small size exhibits unique UV absorbing ability, high stability at high temperatures, high hardness and reactivity as catalyst [5, 6].

Nanoparticles of Cobalt-Manganese oxide and Nickel-Manganese oxide were prepared by chemical co-precipitation method. Doped Cobalt and Nickel oxides show P-type semi conducting behaviour similar to intrinsic spinel Cobalt oxide. Cobalt-Manganese oxide and Nickel-Manganese oxide systems have gained immense importance because of their potential applications such as electrodes in batteries; in solar cells, in super capacitor, in sensors and in switches.

2. EXPERIMENTAL PROCEDURE

Cobalt-Manganese and Nickel-Manganese oxide nanoparticles were prepared by chemical co-precipitation method from analytical grade cobalt sulphate (0.4M), nickel sulphate (0.4M), manganese sulphate (0.4M) and sodium carbonate (0.6M) using ethylene diamene tetra acetic acid as the capping agent. The metal carbonate precipitates were separated from the reaction mixture and washed several times with distilled water and then with ethanol to remove the impurities and traces of EDTA and original reactants if any. The wet precipitates were dried and thoroughly ground using an agate mortar to obtain the metal carbonate precursor in the form of fine powder. On heating to the required temperatures (400, 600 and 800 °C) the metal carbonate precursor decomposes to metal oxides.

2.1 Characterization of the sample

X-ray diffraction is an ideal technique for the determination of crystallite size of the powder samples. The basic principle for such a determination involves precise quantification of the broadening of the diffraction peaks. Based on this principle, a few techniques involving Scherrer equation, integral breadth analysis or Hall-Williamson approach and Fourier method of Warren-Averbach have been developed [7-9]. XRD studies were carried out using XPERT-PRO powder diffractometer (PAN analytical, Netherlands) employing Cu- K_α radiation in the 2θ range 10° to 70° at 30 mA, 40 kV. The TGA/DTA of the nano particles were taken using Perkin-Elmer, Diamond TG/DTA apparatus. The morphologies of the powder samples were characterized by scanning electron microscope (SEM) JEOL/EO JSM-6390. The energy dispersive analyses of X-rays (EDX) were carried out on the samples to ascertain the composition. The infrared spectroscopic (IR) studies of the oxides were made using Perkin-Elmer FTIR spectrophoto meter in the wavenumber range 500 and 4000cm^{-1} by KBr disc method. The UV spectrum were obtained using Shimadzu UV-2550 UV visible spectrophoto meter.

Table 1 – *Table 1a and 1b, variation of particle sizes, elastic strains and optical band gaps of CoMnO and NiMnO nanoparticles prepared at different sintering temperatures*

	Sintering temperature	Particle size (nm)	Elastic strains	Bandgap (eV)
a	400°C	10	0.002305	1.42
	600°C	26	0.000918	1.38
	800°C	31	0.000752	1.30

	Sintering temperature	Particle size (nm)	Elastic strains	Bandgap (eV)
b	400°C	8	0.002620	1.44
	600°C	17	0.001313	1.41
	800°C	41	0.000562	1.37

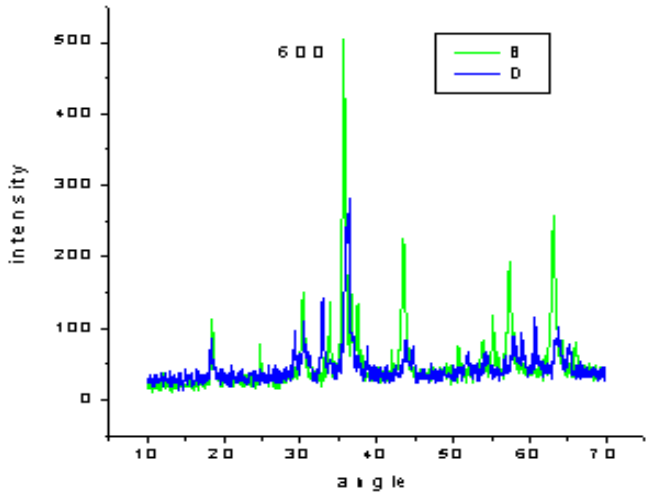

Fig. 1 *– XRD pattern of the CoMnO and NiMnO sintered at* 600 °C

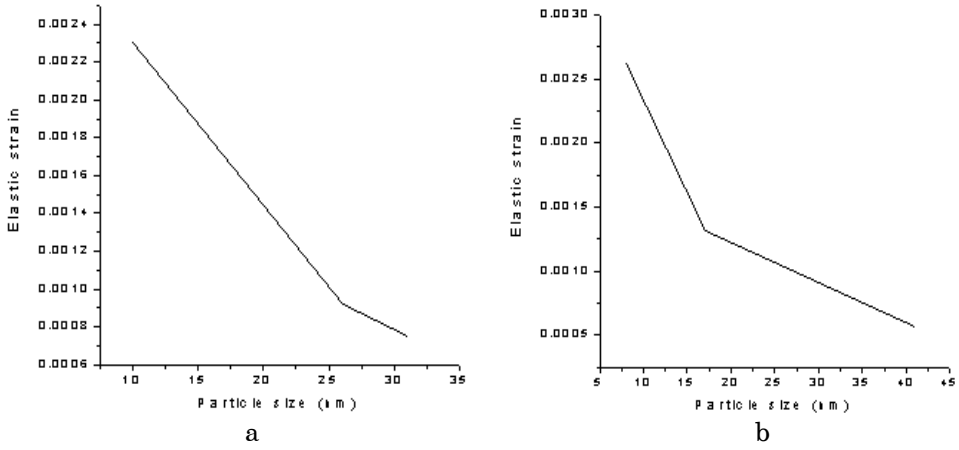

Fig. 2 *– Graph showing variation of elastic strain with particle size for CoMnO (a) and NiMnO (b) nanoparticles*

3. RESULTS AND DISCUSSIONS

3.1 XRD Studies

XRD pattern reveal that the particles are nano sized and crystalline. The particle sizes are calculated from Scherrer equation, $d = 0.9\lambda/\beta\cos\theta$ [10], where β represents the full width at half maximum (FWHM) of XRD lines, $\lambda = 1.54060$ Å. The XRD patterns of CoMnO and NiMnO sintered at 600 °C are shown in Fig. 1. The most intense peaks (intensity 100) are from the (311) planes. The crystallite sizes of CoMnO and NiMnO at various calcination temperatures (400, 600 and 800 °C) are as shown in Table 1a and 1b respectively. As the sintering temperature increases, the particle size increases. This indicates that the size of the crystallites can be adjusted by

controlling the temperature of the reaction [11]. The diffractogram was compared with JCPDS (File No 23-1237 and 01-1110) data to identify the crystallographic phase and cubic structure of the particles. The XRD pattern when compared with JCPDS reveals the structures as spinel oxides. The broadening of the peaks in the XRD pattern may be due to the micro straining of the crystal structures arising from the defects like dislocations and twinning. These are believed to be associated with chemically synthesized nanocrystals. As the crystals grow spontaneously during chemical reaction, the legands get negligible time to diffuse to an energetically favorable site resulting in large crystal defects [12].

The elastic strain of the materials can be calculated using the formula $E = \beta/2 \cot \theta$ [13]. The variation of the elastic strain with particle size is shown in the Fig.2a and 2b. It can be seen that as the particle size increases elastic strain decreases. This strain contributes to the broadening of the XRD pattern.

3.2 Thermal analysis

Thermo gravimetric analysis of the carbonate precursor was carried out to determine the decomposition temperature and the rate of decomposition. The decomposition temperature is found to lie between 300 and 350 °C. Thus the heat treatment of the ground precursor powders at their respective decomposition temperature and beyond results in the evolution of heat from the combustion of the residual carbonaceous material. This facilitates the reaction among the constituent metal ions and the formation of the desired oxide phase at relatively low external temperature.

3.3 Micro structural studies

For the micro structural studies, the samples heated at 600°C were directly transferred in to the chamber of the SEM with out disturbing the original nature of the products. SEM images and the energy dispersive spectra (EDX) of CoMnO and NiMnO are shown in the Fig. 3a, 3b and 4a, 4b respectively. The SEM pictures reveal that the particles are more or less spherical in shape.

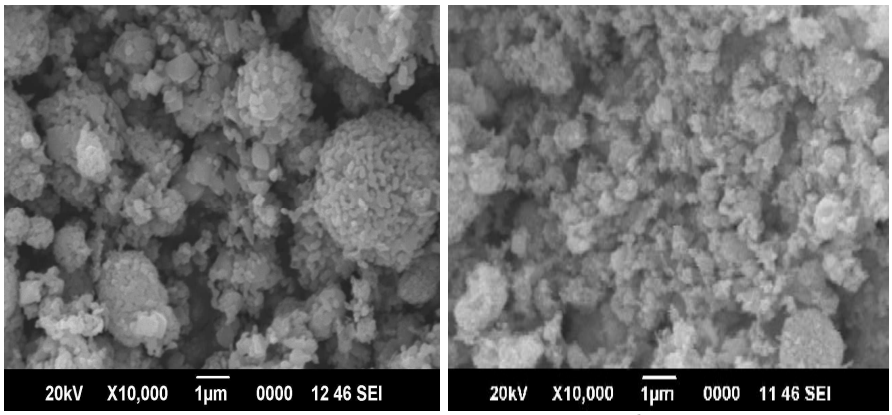

a b

Fig. 3 *– SEM image of CoMnO (a) and NiMnO (b)*

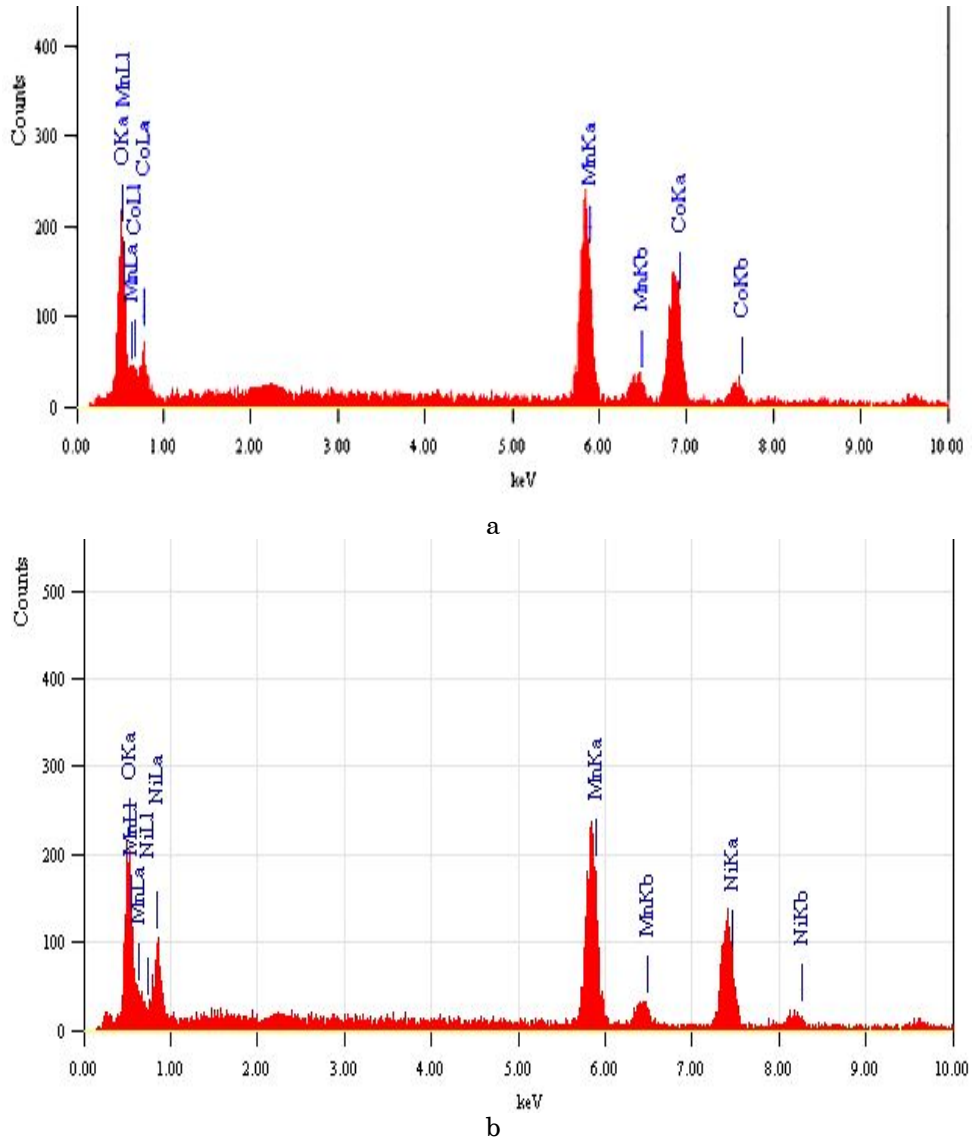

Fig. 4 *– EDX spectrum of CoMnO (a) and NiMnO (b)*

3.4 FTIR Spectra analysis

The FTIR spectra of the samples are shown in Fig. 5a and 5b respectively. The broad absorption bands in the region around 3390 and 3420 cm^{-1} are due to the presence of co-ordinated / entrapped water. The presence of some carbonaceous materials is evident from the IR spectra which depicts the bands at 1630 and 1640 cm^{-1} corresponding to carboxylate ions [14, 15]. The band around 600cm^{-1} may be due to the bending modes of the metal oxides. The other bands may be due to the micro structural formation of the samples.

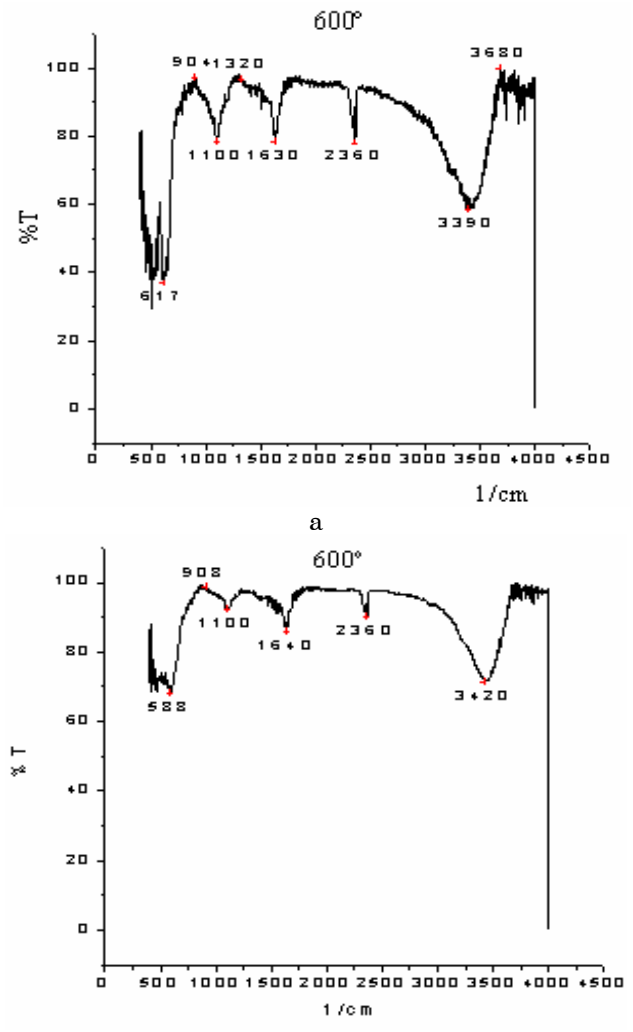

a

b

Fig. 5 *– FTIR spectrum of CoMnO (a) and NiMnO (b)*

3.5 UV spectral studies

The UV spectra of CoMnO and NiMnO sintered at 400, 600 and 800 °C are taken in the wavelength range of 200 to 800 nm with 1 nm resolution is shown in fig 6a and 6b respectively. UV spectra provide important information about the details related with optical band gap of the material. The energy band of the material is related to the absorption coefficient α by the Tauc relation, $\alpha h\nu = A(h\nu - E_g)^n$, where A is a constant, hυ is the photon energy ($\nu = c/\lambda$), Eg is the band gap and $n = 1/2$ for an allowed direct transition. Plotting a graph between $(\alpha h\nu)^2$ and $h\nu$ (Fig. 7) gives the value of direct band gap of CoMnO and NiMnO sintered at 600 °C [16]. The

extrapolation of the straight line to $(\alpha h\nu)^2 = 0$, gives the value of the band gap. From the UV spectra, it is clear that the absorbance decreases with increase in wavelength. This decrease in the absorption indicates the presence of optical band gap in the material. This corresponds to the excitation of surface plasmons in the composite nano particles. The optical band gap of the materials determined from the absorption spectra is shown in the Table 1. As the sintering temperature increases, the particle size increases and the band gap decreases.

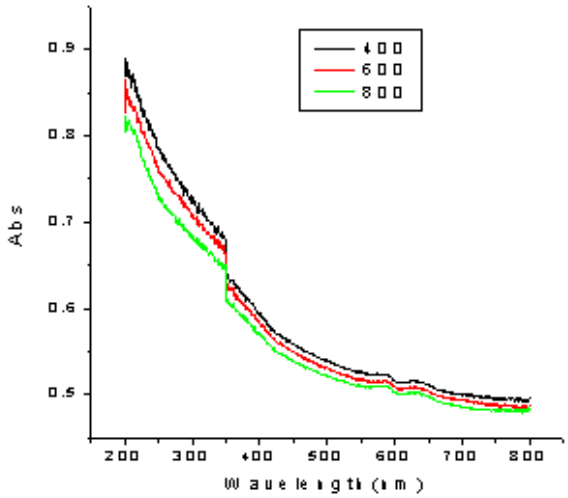

a

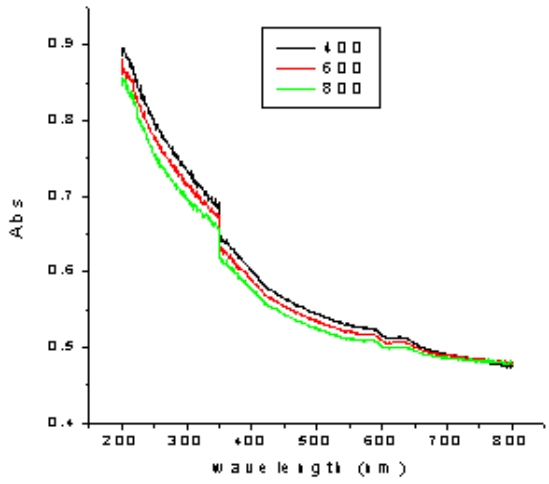

b

Fig. 6 – *Absorbance versus wavelength graphs for CoMnO (a) and NiMnO (b) at* 400, 600 *and* 800 °C

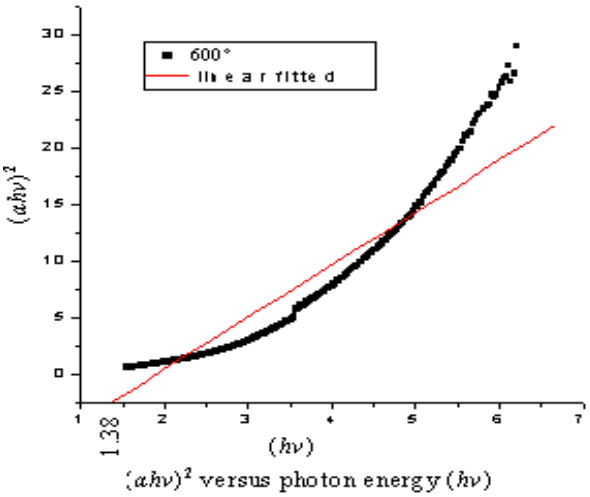

a

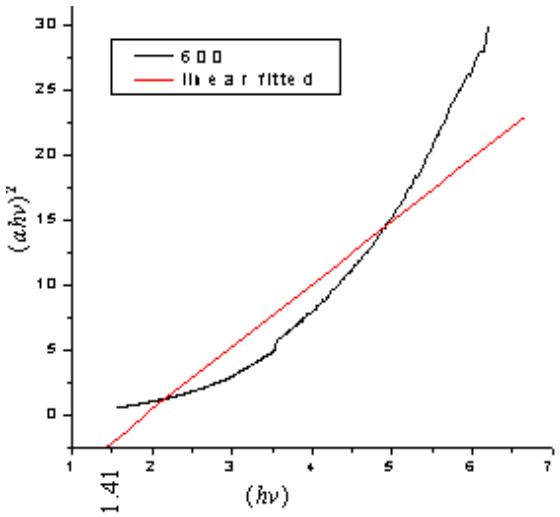

b

Fig. 7 *– $(\alpha h\nu)^2$ versus $h\upsilon$ graphs for the samples sintered at* 600 °C

REFERENCES

1. R. Lopez, T.E. Haynes, L.A. Boatner and R.F. Haglund, *Opt. Lett.* **27,** 1327 (2002).
2. M. Ikeyama, S. Nakao, M. Tazawa, K. Kamada, *Nucl. Instrum. Meth. B* **175,** 652 (2001).
3. M. Muroi, R. Street, P.G. McCormick, *J. Appl. Phys.* **87,** 3424 (2000).
4. Kenneth J Klabunde & Cathymohs, Department of Chemistry, Kansas state university, *Manhanttan Kansas second Edition*: 1998).
5. M.S. Tsai, *Mater. Sci. Eng. B.* **110,** 132 (2004).
6. T. Mori, Y.R. Wang, J. Drennan, *Solid State Ionics* **175,** 641 (2004).
7. P. Scherrer, *Math. Phys. K.* **1**, 98 (1918).

8. G.K. Williamson, W.H. Hall, *Acta Metall.* **1**, 22 (1953).
9. B.E. Warren, B.L. Averbach, *J. Appl. Phys.* **21**, 595 (1950).
10. B.D. Cullity, *Elements of X-ray diffraction*, (Addison-Wesley publishing company, Inc. California: 1970).
11. L.P. Wang, G.Y. Hong, S.C. Qu, Z.G. Wang, *Nanotechnology* **16**, 1469 (2005).
12. H.C. Warad, S.C. Ghosh, Hemtanon, *Sci. Technol. Adv. Mater.* **6**, 296 (2005).
13. R. Kelsall, I. Hamley, M. Geoghegan, *Nano Scale Science & Technology*, (John Wiley: Chichester: 2005).
14. G. Ehrlich, *J. Am. Chem. Soc.* **76**, 5263 (1954).
15. F. Douville, G. Duval & J. Lecomte, *Compt. Rend. Acad. Sci.* **212**, 963 (1941).
16. D. Mohanta, S.S. Nath, N.C. Mishra, A. Choudhury, *Bull. Mater. Sci.* **26**, 289 (2003).